

Estimating CaCO₃ Content Based on Natural Gamma Ray (NGR) in Deep-Ocean Sediment Cores

Alina Shchepetkina^{1,*}, Paul Moal-Darrigade², Stephen Pekar³, Trevor Williams⁴ and the South Atlantic Transect IODP Expedition 390 & 393 Scientists

¹University of Western Ontario, Department of Earth Sciences, London, ON, Canada

²Univ. Bordeaux, CNRS, EPHE, INP, EPOC, UMR 5805, F-33600 Pessac, France

³School of Earth and Environmental Sciences, Queens College, Flushing, NY 11367, USA

⁴International Ocean Discovery Program, Texas A&M University, College Station, TX, USA

*Corresponding author email: ashchep@uwo.ca

ABSTRACT: We present a simple, quick, and high-resolution (approx. 10 cm) method for calculating almost continuous calcium carbonate (CaCO₃) proxy records in deep-marine sediment cores based on the well-known dependence of NGR (natural gamma ray) on sediment clay content. The method used in this study is based on the assumption that sediment composition along the SAT (South Atlantic Transect) consists of two components: carbonate and clay. This assumption is reasonably accurate for the region under investigation. At carbonate-rich Site U1583 (66–97 wt% CaCO₃), calculated CaCO₃ wt% contents are within 4.18% at 1 standard deviation (σ) of geochemical analyses of the CaCO₃ wt% contents of discrete samples (measured using a coulometer), while at the more lithologically variable Site U1557 (0.1–92 wt% CaCO₃), they are within 15.6% at 1 σ . Results indicate good to excellent correlations between the NGR- and coulometry-derived datasets, supporting the use of this method for carbonate stratigraphy, paleoceanography, and paleoclimate reconstructions. We provide an equation to derive CaCO₃ wt% from NGR based on the SAT datasets. The procedure described below can be used to construct the higher resolution proxy CaCO₃ records at other sites worldwide compared to discrete CaCO₃ values. This method can assist with shipboard lithology determination and can guide core sampling.

Keywords: International Ocean Discovery Program, JOIDES Resolution, South Atlantic Transect, Paleoceanography, Carbonate Compensation Depth (CCD), deep ocean

INTRODUCTION

Temporal variations in CaCO₃ (calcium carbonate) records from deep-sea sites provide essential insights into stratigraphy, paleoceanography, and paleoclimatology at both long and short timescales throughout the Cenozoic Era (Dadey and Lyle 1995; Lindsey and Schellenberg 2006; Mayer 1991). At abyssal depths, changes in the CaCO₃ content of sediments may reflect changes in the depth of the lysocline and CCD (carbonate compensation depth), which may reflect changes in water masses, carbonate productivity, and/or atmospheric CO₂ (e.g., Berger 1972; Dutkiewicz and Müller 2021; Farrell and Prell 1989; Lyle et al. 1988; Melguen 1978; Pedersen 1983; Van Andel 1975). The most extensive long-term records of CaCO₃ content have been developed from sediment samples collected from 50+ years of scientific ocean drilling conducted by the IODP (International Ocean Discovery Program) and its predecessors (e.g., Becker et al. 2019). Solid-phase geochemical measurements (CaCO₃ wt%) are typically conducted on discrete samples of sediment cores that are taken shipboard and analyzed using a coulometer either during the expedition or post-expedition. This work destroys the sample and is both time-consuming and expensive, and, as a result, shipboard geochemical analyses are usually low resolution, normally 1–2 samples per core (i.e., every 5–10 m).

Lithologic descriptions of deep-ocean cores onboard the *JOIDES Resolution* rely on macroscopic and microscopic observations to establish the primary sediment types by the identification of major and minor lithologies that often predominantly include biogenic CaCO₃ and detrital clay (Marsaglia et al. 2013, 2015; Mazzullo

and Graham 1988; Phillips and Littler 2022). Even though smear slides allow the accurate identification of the major bioclastic components of the sediments (e.g., nannofossils, foraminifers, diatoms), the components of the clay-size fraction often cannot be properly estimated (c.f. Phillips and Littler 2022). Such estimation errors result from differing levels of expertise of the shipboard petrographers, the preponderance of very fine-grained bioclastic components (e.g., nannofossils) which mask the clay particles, and varying smear-slide preparation techniques, where thick nannofossil ooze might resemble clay clumps (Marsaglia et al. 2015). A reliable high-resolution estimate of carbonate content would enable more precise lithological descriptions, especially of fine-grained sediments.

In petrophysics, it is standard practice to use NGR (natural gamma radiation) to estimate shale volume (synonymous with clay volume) (e.g., Section 1.1 in https://wiki.aapg.org/Standard_interpretation; Telford et al. 1976; Rider 1996). This method relies on radioactive isotopes of K (potassium) and Th (thorium) that are relatively common in clay minerals compared to most other major rock-forming minerals: the greater the clay content, the higher the NGR value. It also assumes that other sources of NGR are minor, for example even though high NGR has been reported from phosphatic shell and bone material that has high U (uranium) content, these occurrences are common in oceanic upwelling zones and offshore, but are not found in deep sea (Burnett et al. 1983; Kochenov and Baturin 2002; Veeh et al. 1974). In sediments composed predominantly of two components (i.e., clay-carbonate sediments), the

non-clay component is carbonate, thus can also be quantified: the lower the NGR value, the higher the carbonate content. Where CaCO_3 coulometer measurements from samples of the same cores are available, the inverse of the NGR value can be scaled to estimate the $\text{CaCO}_3\%$ content.

On the *JOIDES Resolution*, NGR is measured in the physical properties laboratory on a one-of-a-kind NGR measurement system installed in 2009 with the large-scale renovation of the ship as part of the Scientific Ocean Drilling Vessel (SODV) project (Vasiliev et al. 2011), building on previous IODP (and its predecessors) NGR instruments and paleoceanographic applications (Rothwell and Rack 2006). NGR has been used qualitatively on previous IODP expeditions either as a proxy for CaCO_3 when inversely correlated to ICP-OES (Inductively Coupled Plasma Optical Emission Spectroscopy)-determined CaCO_3 concentrations (Lindsey and Schellenberg 2006) or as a proxy for clay using the downcore trends in NGR (Phillips and Littler 2022). Other physical properties data collected on IODP expeditions that have also been used as a proxy for clay and CaCO_3 content include GRA (gamma-ray attenuation density; Mayer 1991; Walczak et al. 2015), color reflectance (Millwood et al. 2002), and RGB blue channel (Lamy et al. 2019). Moreover, there have been a few attempts to calculate CaCO_3 content onboard IODP expeditions using a Schlumberger downhole active-source gamma-ray spectrometry tool to obtain Ca concentrations (Dadey and Lyle 1995; Pratson et al. 1992a, 1992b, 1993). The conversion from elemental Ca to CaCO_3 was accomplished using oxide factors. However, the method produced results that were consistently lower than the coulometry-derived CaCO_3 measurements.

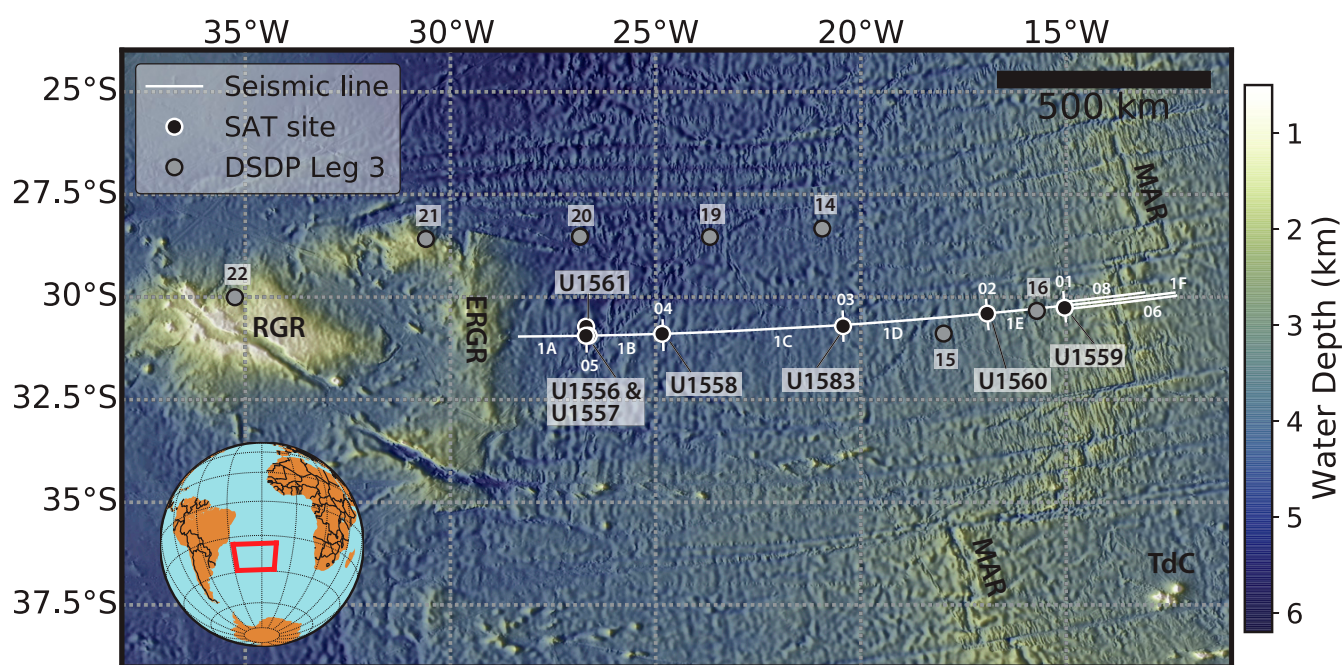
In all aforementioned physical property-based CaCO_3 proxy approaches, the data records are effectively continuous (compared with discrete sample-based CaCO_3 measurements) and span the

whole length of the borehole. Therefore, if a process can be developed to convert NGR data to CaCO_3 content estimates with minimal data processing, high-resolution CaCO_3 records could be generated far more efficiently than through geochemical analysis. In previous attempts to calibrate physical property records to CaCO_3 content, limitations arose in binary sedimentary systems (i.e., CaCO_3 and detrital terrigenous material) with high clay concentrations and widely varying clay mineral types (Dadey and Lyle 1995). The previous work was mostly used as a qualitative measure of carbonate content or lithology. Surprisingly, to our knowledge, there has not yet been a published method to derive quantitative physical-property-based CaCO_3 records from NGR measurements, together with an error assessment and discussion of which deep-sea sediments it can be applied to.

Here, we present a method of estimating CaCO_3 content by calibrating NGR data to laboratory measurements of CaCO_3 content after converting to mass-normalized NGR values using GRA density measurements. The CaCO_3 calibration can also potentially be applied to downhole wireline logs for non-cored holes or holes with poor core recovery (Dadey and Lyle 1995), permitting better correlations between the holes of the same site or between various sites in real time.

OCEANOGRAPHIC SETTING

IODP SAT (South Atlantic Transect) Expeditions 390C, 395E, 390, and 393 obtained deep-ocean sediment cores at seven sites in water depths ranging from approx. 3055 to 5006 m and forming a transect at $\sim 31^\circ\text{S}$, located 130–1250 km westward from the Mid-Atlantic Ridge (text-figure 1, Table 1; Coggon et al. 2020, 2022a, 2022b; Estes et al. 2020; Williams et al. 2021; Teagle et al. 2023). These expeditions recovered sedimentary sections up to 564 m thick overlying 6.6–61.2 Ma oceanic crust produced at slow to intermediate spreading rates (Table 1; Estes et al. 2020; Williams et al. 2021;



TEXT-FIGURE 1

Bathymetric map of the study sites with the main tectonic features and drill sites of the SAT (South Atlantic Transect; white line) (Teagle et al., 2023).

TABLE 1
South Atlantic Transect (SAT) sites with coordinates, distance from the Mid-Atlantic Ridge, estimated crustal age (Ma), and water depth (m).

IODP Site	Hole	Latitude,°	Longitude,°	Distance from Mid-Atlantic Ridge, km	Crustal age, Ma	Water depth, m
U1559	B	30°15.6336'S	15°2.0941'W	130	6.6	3055
U1560	B	30°24.2057'S	16°55.3702'W	315	15.2	3723
U1583	F	30°42.6175'S	20°26.0336'W	652	30.6	4210
U1558	D	30°53.7814'S	24°50.4822'W	1067	49.2	4334
U1557	D	30°56.4651'S	26°37.7892'W	1243	60.7	5011
U1556	B	30°56.5244'S	26°41.9472'W	1250	61.2	5002

Coggon et al. 2022b; Teagle et al. 2023). One of the main goals of these expeditions was to reconstruct the history of deep water-masses in the western South Atlantic Ocean over the past 61 My (Coggon et al. 2020, 2022a). The development of a continuous and high-resolution record of carbonate deposition is an essential first step to studies of the CCD, microfossil preservation, and how they all relate to global carbon cycling and ocean circulation.

METHODS

Soon after sediment cores were recovered from the ocean floor using the APC (advanced piston corer) or the XCB (extended core barrel) system and then curated, the whole-round core sections were analyzed on the STMSL (Special-Task Multisensor Logger) to obtain the GRA bulk density (g/cm^3) and the NGRL (Natural Gamma Ray Logger) to obtain the NGR readings (counts per second;

TABLE 2
Comparison of the effectiveness of the new method for South Atlantic Transect (SAT) holes: μ —average estimation error; M—median estimation error; σ —standard deviation of estimation error from coulometry-derived CaCO_3 values.

Hole	Metrics	This study
U1556A	μ	0.00
	M	−1.25
	σ	11.88
U1556C	μ	−1.42
	M	−1.58
	σ	16.62
U1557B	μ	−4.51
	M	−2.29
	σ	16.20
U1558A	μ	−0.54
	M	−0.39
	σ	4.08
U1558F	μ	1.57
	M	0.68
	σ	7.02
U1559A	μ	−0.85
	M	−1.03
	σ	2.25
U1560A	μ	−2.26
	M	−0.37
	σ	1.43
U1583C	μ	−2.06
	M	−2.57
	σ	4.18

cps). GRA measurements were taken every 2.5 cm during the SAT expeditions. NGR measurements integrated gamma radiation from an approx. 10 cm interval of core, because the sensors on the NGRL are 10 cm wide, with the measurement assigned to the midpoint depth of that 10 cm interval. Once the cores were split, the sedimentologists chose 1–2 samples per core from the working half for CaCO_3 content analysis to capture variations in lithological composition. Traditionally, the CaCO_3 content of marine sediments is determined by pressure calcimeter or coulometric techniques (Chaney et al. 1982; Engleman et al. 1985; Huffman 1977; Jones and Kaiteris 1983; Pimmel and Claypool 2001). These same techniques were employed during the SAT expeditions to assess the CaCO_3 content in the sediment samples. These coulometry-derived CaCO_3 measurements were used as the standard against which all NGR-based estimates were compared. All data processing was conducted in Excel. The standard physical properties data (i.e., NGR in cps, GRA, MAD (moisture and density)) and standard carbonate chemical data (i.e., CaCO_3 in wt%) vs. depth were downloaded and pre-filtered (i.e., deleted measurements of repetitive runs, outlier values, and gaps in core recovery) from the LIMS (Laboratory Information Management Systems) Reports database.

Herein, we present two methods for estimating the CaCO_3 content using NGR data in sediment cores (in each case, 1 standard deviation (σ) of CaCO_3 contents was calculated using the difference between the CaCO_3 values obtained from onboard coulometry and the high-resolution estimates of CaCO_3 from the linear regression). The first method (Simple NGR Proxy) is simple and quick, providing a good visual match to the coulometry-derived CaCO_3 data in relatively homogenous sediments with high CaCO_3 content (>60%; e.g., Sites U1558, U1559, U1583, U1560). When coulometry-derived CaCO_3 content (wt%) is plotted vs. NGR (cps), an inverse, approximately linear relationship is observed between the two data sets, and the NGR values can be scaled to CaCO_3 accordingly. However, in this method, NGR data are not corrected for downhole density changes due to compaction or lithology. Neither are they corrected for the geometry of the core (e.g., incompletely filled core liners, cracks, and voids). The second method (Density-corrected NGR Proxy) accounts for these changes, normalizing by GRA density, based on the method described by Walczak et al. (2015). Similarly, whenever there are sediment gaps or the cross-sectional area of the sample changes much (as may be the case of a rotary drilled core, XCB), normalization by GRA density compensates for this to a certain extent.

SIMPLE NGR PROXY

CaCO_3 content measurements tend to be sparse compared to NGR measurements, which have a 10-cm spacing, hence, only a few

data points are available for correlation. Therefore, the depth of an NGR value often does not match the exact depth of a CaCO₃ content value. A simple method to account for this is to manually assign CaCO₃ content to the NGR value that is closest to it in depth (see text-figure 2A and 3A as examples for Sites U1583C and U1557B). However, this method can introduce minor errors as NGR values may be offset by up to 5 cm from the depths of CaCO₃ analyses and, thus, may have slightly different values from where the CaCO₃ content sample was collected. To account for this, we used a modified method, where we interpolated between adjacent NGR values to match the CaCO₃ content sampling depths using linear interpolation for untabulated points, i.e., the Excel Forecast function (see Dagra Data Digitizer 2022). Linear interpolation estimates the value of a property at a point intermediate to two points with known values, assuming a linear trend between them (Eq. 1):

$$(1) \text{ NGR} = \text{NGR}_1 + (D - D_1) \frac{(\text{NGR}_2 - \text{NGR}_1)}{(D_2 - D_1)}$$

where the interpolated NGR value at depth D is located between adjacent NGR depths D_1 and D_2 with NGR values NGR_1 and NGR_2 , respectively.

Upon obtaining the interpolated NGR values that match the CaCO₃ content sampling depths, we plotted them against the coulometry-derived CaCO₃ content data (see text-figures 2B, 3B as examples for Sites U1583C and U1557B). The obtained linear regression between the plotted values provided us with two parameters: the linear trendline and R-squared value (R^2 — a goodness-of-fit indicator for linear regression models: the closer the value to 1, the better the fit). CaCO₃ content (see text-figures 2D-E for Site U1583C and text-figures 3D-E for Site U1557B) was then calculated using the linear regression equation. Depending on the preferred method, a user can “feed” either 1) manually matched NGR counts using Eq. 2a as an example for Site U1583C (text-figure 2A) or Eq. 2b as an example for Site U1557B (text-figure 3A) or 2) interpolated NGR counts using Eq. 3a as an example for Site U1583C (text-figure 2B) or Eq. 3b as an example for Site U1557B (text-figure 3B) to obtain the linear regression equation. These two variants of the Simple NGR proxy give very similar results. Such CaCO₃ proxy data derived from NGR data have a resolution of approx. 10 cm:

$$(2a) \text{ CaCO}_3 = -2.6578 \cdot \text{NGR} + 100 \quad (R^2 = 0.96)$$

$$(2b) \text{ CaCO}_3 = -2.3967 \cdot \text{NGR} + 100 \quad (R^2 = 0.73)$$

$$(3a) \text{ CaCO}_3 = -2.6116 \cdot \text{NGR} + 100 \quad (R^2 = 0.95)$$

$$(3b) \text{ CaCO}_3 = -2.4531 \cdot \text{NGR} + 100 \quad (R^2 = 0.75)$$

where the CaCO₃ content is in wt%, and the NGR values are in cps.

DENSITY-CORRECTED NGR PROXY

To create a more accurate CaCO₃ content record using the NGR data, the density-corrected NGR proxy method was implemented. The need for this method arises from the fact that NGR data are collected in counts per second (cps) over a constant volume, whereas coulometry-derived CaCO₃ measurements are reported as standard

carbonate chemical data in wt%. Given variations in the density of the sediments, the two data types are not directly comparable. Consequently, additional steps are needed to convert the NGR data so that they are also reported relative to sediment mass, rather than volume. This problem becomes more acute in cores where the density varies widely. For example, in clay-rich sediment compositions (e.g., clay is >20% of the dry sediment), more compacted sediments would have higher NGR values than less compacted sediments because more tightly packed clays contain more radiogenic elements per unit volume. In the context of the SAT holes, the issue arises in binary systems (clay- or carbonate-rich), where carbonate varies between low (<40 wt%) and high (>97 wt%), resulting in bimodal sediment density. To account for such highly varying lithologies, as is the case at SAT Sites U1556 and U1557, where the sediments alternate between almost pure clay and pure nannofossil ooze, we corrected for density changes by transforming the total NGR counts (cps) measured per volume of sediment (cm³) into total NGR counts (cps) measured per dry sediment mass (g). To transform the NGR values from cps to cps/g, we divided them by the dry bulk density, which was calculated using the GRA-derived bulk density (g/cm³) together with the grain density, calculated porosity, and dry bulk density measured on discrete samples (see the procedure below).

First, we performed quality control on the GRA data, laboratory-measured dry bulk density, grain density, calculated porosity, and calculated dry bulk density measurements. We deleted any data points associated with 1) double or triple measurements over the same interval; 2) clasts of basement in the sediment section; 3) spurious bulk density values of <1.03 g/cm³, which reflect intervals with very little or no sediment that might be associated with gaps in core recovery (e.g., at the ends of the 1.5-m-long core sections, in cracks related to a drilling technique, or in the core catcher section) and/or gas expansion; and 4) intervals with intense drilling disturbance.

Second, the corrected total NGR counts per sediment mass (cps/g) were calculated as follows:

1) we applied 5-point (10 cm) averaging to GRA data (i.e., simple moving average smoothing) to make the resolution closer to the NGR dataset and to reduce the variance in the data. Alternatively, a user might apply a 20-cm Gaussian smoothing following Walczak et al. (2015);

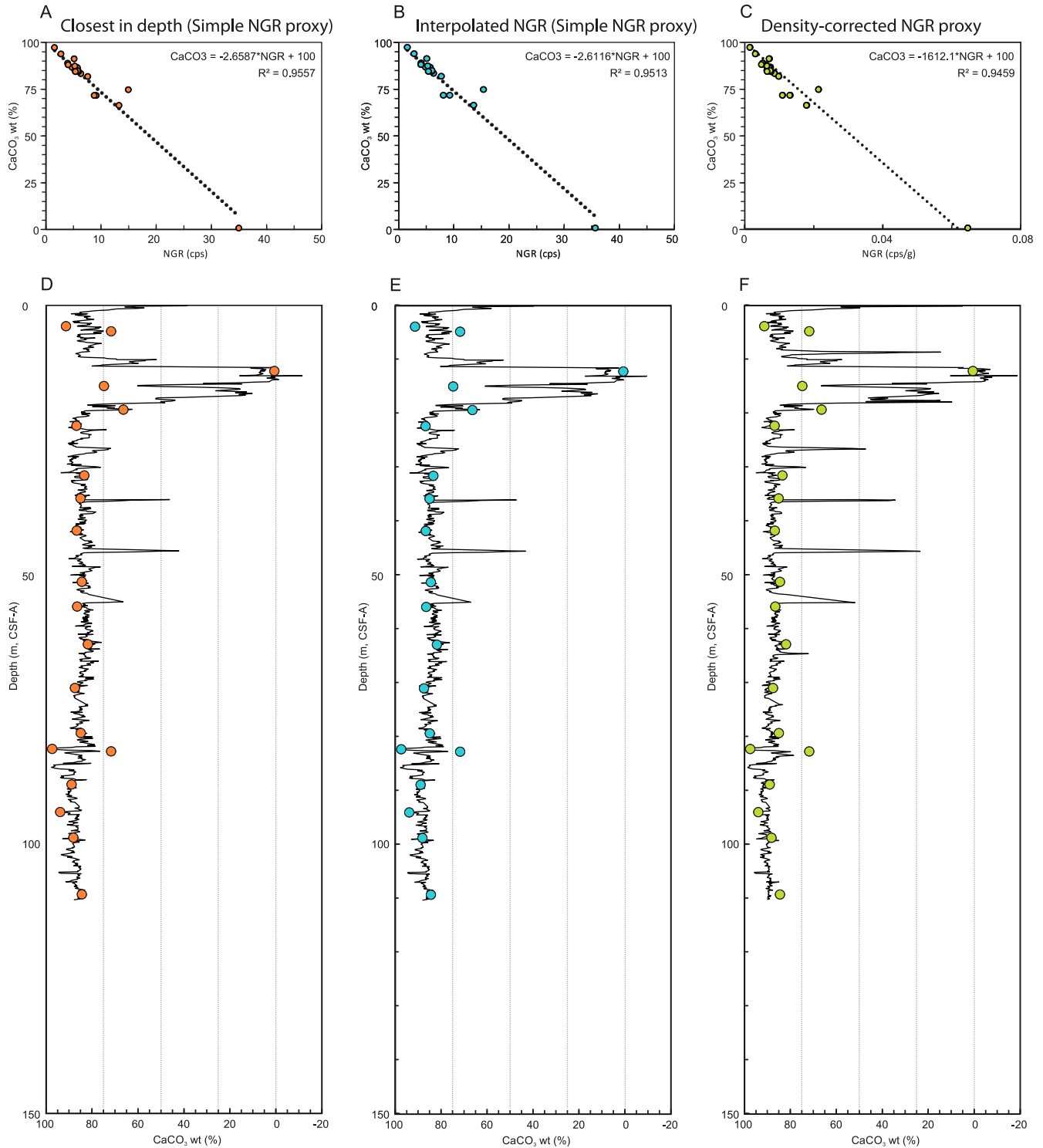
2) interpolated averaged GRA values to the NGR sampling depths (i.e., approx. every 10 cm);

3) calculated the median grain density value (σ_g) for each hole using the Excel function MEDIAN (grain densities are part of the suite of “moisture and density” values measured on sediment samples during the expedition (Coggon et al. 2022b; Teagle et al. 2023);

4) assumed the density of pore water (σ_w). For this study, we used $\sigma_w = 1.03 \text{ g/cm}^3$ to approximate the density of seawater;

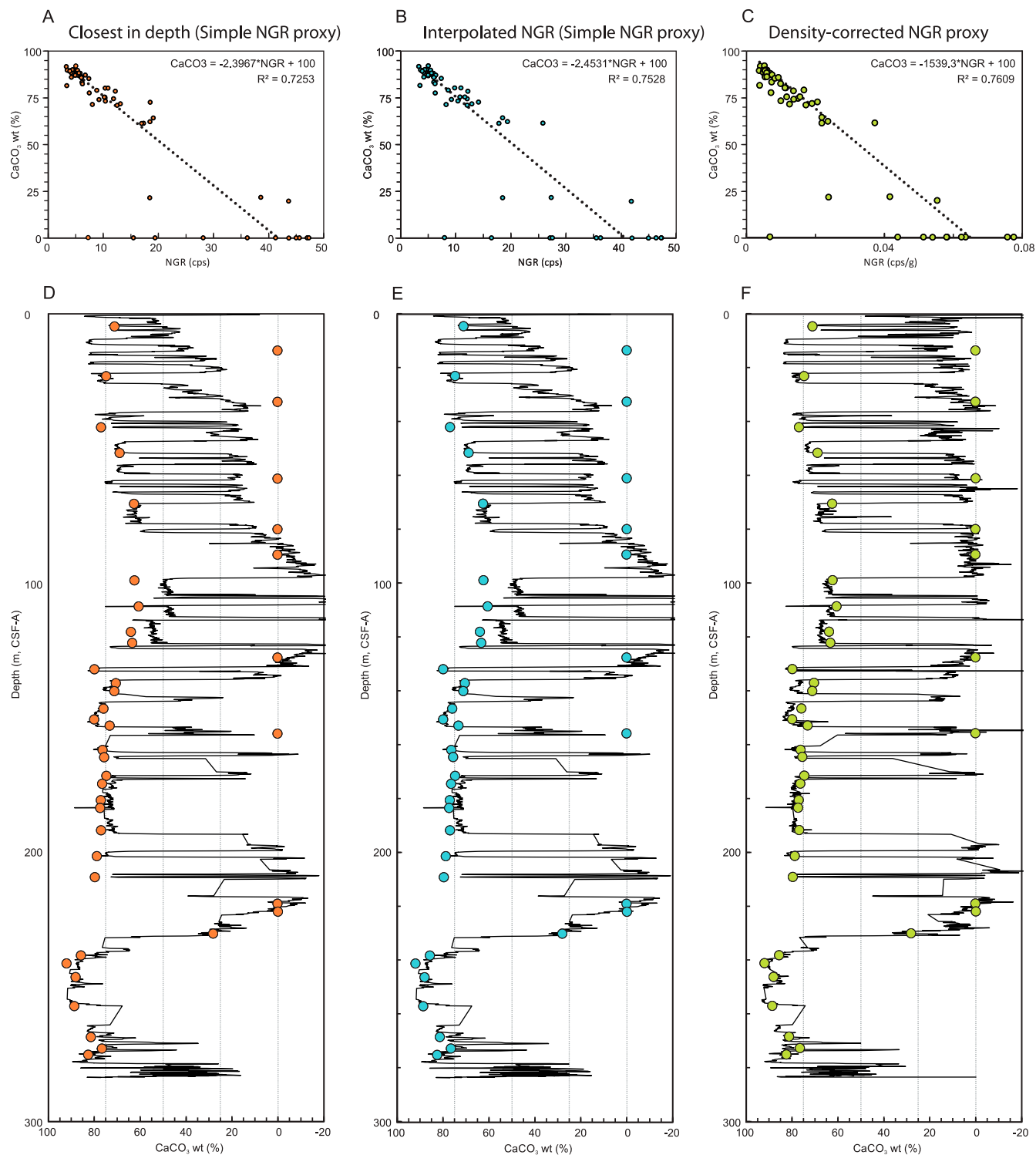
5) calculated sediment porosity (Φ ; Eq. 4), filtering out potentially erroneous, averaged GRA bulk sediment densities of less than 1.2 g/cm^3 ;

$$(4) \Phi = 100 - \left(100 \cdot \frac{(\sigma_b - \sigma_w)}{(\sigma_g - \sigma_w)} \right)$$



TEXT-FIGURE 2

(A–C) Cross-plots of coulometry-derived CaCO_3 content (wt%) vs. NGR counts for Hole U1583C with linear regression equation and R^2 value. (A) NGR in counts per second per volume (cps) manually assigned to the closest CaCO_3 content analysis depth. (B) NGR in cps interpolated to CaCO_3 content analysis depths using the Excel Forecast function. (C) Calculated NGR in cps/g. (D–F) NGR-based CaCO_3 content (wt%) records synthesized from the application of three different NGR– CaCO_3 content calibrations (A–C) to the approx. 10 cm resolution NGR record of Hole U1583C.



TEXT-FIGURE 3

(A–C) Cross-plots of coulometry-derived CaCO_3 content (wt%) vs. NGR counts for Hole U1557B with linear regression equation and R^2 value. (A) NGR in counts per second per volume (cps) manually assigned to the closest CaCO_3 content analysis depth. (B) NGR in cps interpolated to CaCO_3 content analysis depths using the Excel Forecast function. (C) Calculated NGR in cps/g. (D–F) NGR-based CaCO_3 content (wt%) record synthesized from the application of three different NGR– CaCO_3 content (wt%) calibrations (A–C) to the approx. 10-cm-resolution NGR record of Hole U1557B.

where σ_b is the averaged GRA bulk sediment density (g/cm^3) interpolated to NGR sampling depths (i.e., approx. every 10 cm); σ_g is the median grain density (g/cm^3) for each hole; and σ_w is the assumed density of pore water (1.03 g/cm^3). Note that this method relies on the fact that the grain densities of calcite (2.71 g/cm^3) and clay (a range, but average approx. 2.7 g/cm^3) are similar to each other. This method is not appropriate for intervals containing components with other, radically different densities (e.g., biogenic silica);

6) calculated dry bulk sediment density (g/cm^3 ; Eq. 5) for the core at NGR sampling depths (i.e., approx. every 10 cm):

$$(5) \sigma_{db} = \sigma_g * \left(1 - \left(\frac{\Phi}{100}\right)\right)$$

where σ_{db} is the dry bulk sediment density (g/cm^3); σ_g and Φ are as above.

7) Finally, we calculated total NGR counts per mass (cps/g; NGRd) as follows:

$$(6) \text{NGRd} = (\text{NGRv}/V_s)/(\sigma_{db})$$

where NGRv is the total NGR counts per second per volume (cps); V_s is the sample volume (for *JOIDES Resolution* cores analyzed in the NGRl, $V_s = 655 \text{ cm}^3$ (Vasiliev et al. 2011)); and σ_{db} is the dry bulk sediment density (g/cm^3) (Eq. 5).

Similarly to the Simple NGR Proxy method, we interpolated the NGRd values to match the depths from which discrete samples were taken for coulometry-derived CaCO_3 content analyses. Linear regression between the NGR values (cps/g) and the coulometry-derived CaCO_3 values (wt%) provided linear trendlines described by Eq. 7a and Eq. 7b (see text-figures 2C, 3C as examples for sites U1583C and U1557B, respectively), whereas the correlation coefficient (R^2) described the strength of the correlation between those two variables. The linear regression equation was then used to calculate the proxy CaCO_3 contents (in wt%) from NGR data throughout each hole (approx. every 10 cm; see text-figures 2F, 3F for Sites U1583C and U1557B, respectively).

$$(7a) \text{CaCO}_3 = -1612.1 * \text{NGR} + 100 \quad (R^2 = 0.95)$$

$$(7b) \text{CaCO}_3 = -1539.3 * \text{NGR} + 100 \quad (R^2 = 0.76)$$

where the CaCO_3 content is in wt%, and the NGR values are in cps/g.

RESULTS AND INTERPRETATIONS

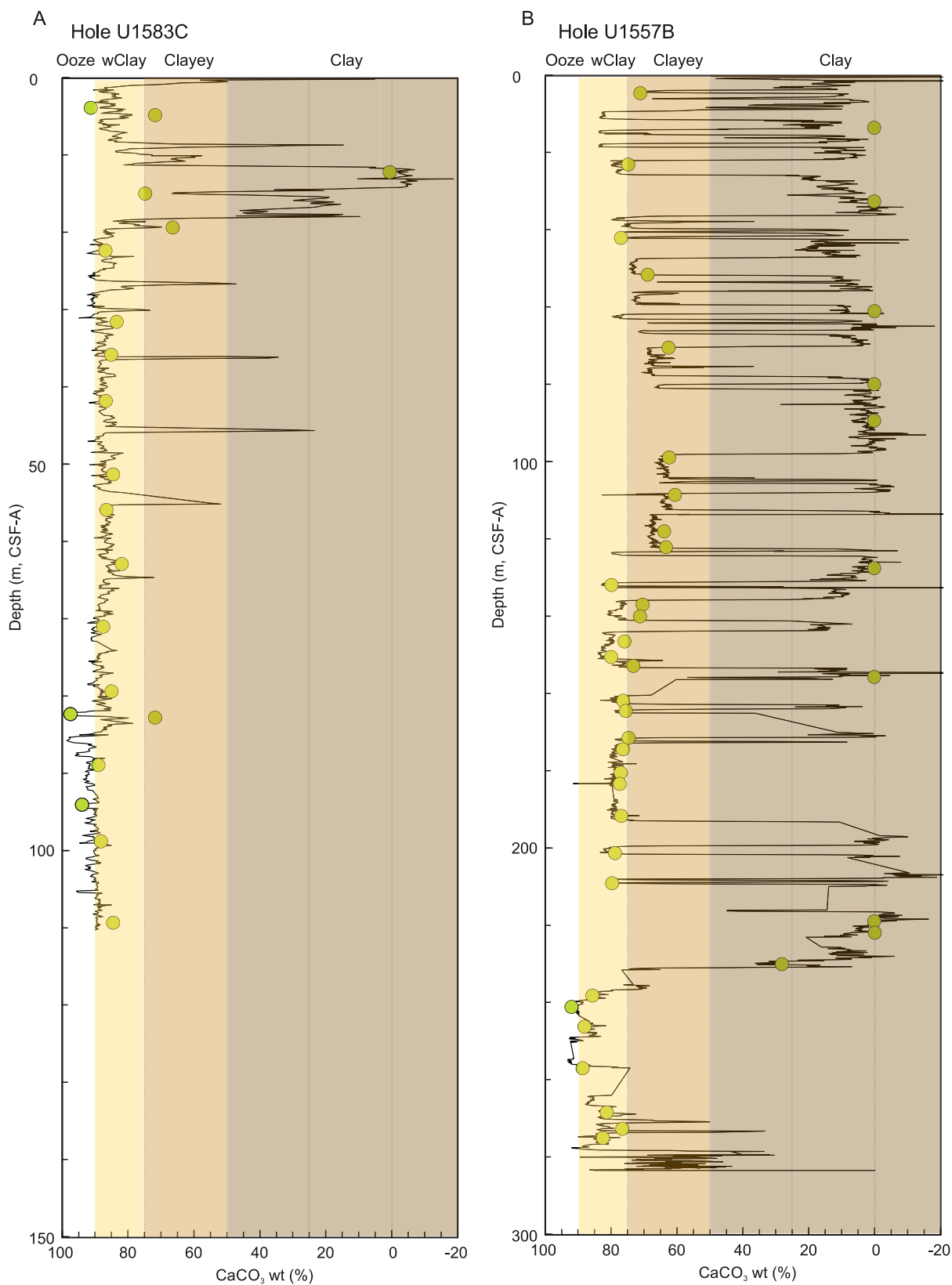
The methods described above were implemented to reconstruct high-resolution CaCO_3 stratigraphy for seven IODP sites in the South Atlantic Ocean at $\sim 31^\circ\text{S}$ (text-figure 1). The data from two representative sites (U1583 and U1557) demonstrate the practical application of this method (see Appendix for cross-plots of other SAT holes). Both sites are located in the South Atlantic gyre and, therefore, are characterized by low sedimentation rates (approx. $0.5\text{--}1.5 \text{ cm/kyr}$; Coggon et al. 2020, 2022b; Estes et al. 2020; Teagle et al. 2023) and contrasting lithological trends and total thicknesses (106 and 564 m, respectively). Site U1583,

located on 30.6 Ma crust, remained above the CCD for its entire history and is characterized by relatively homogenous sediments comprising nannofossil ooze with varying amounts of clay, where the CaCO_3 content does not fall below 70 wt% (except one clay level with 0.64 wt% CaCO_3) and never goes above 97 wt%. In contrast, Site U1557, located on 60.7 Ma crust, was below the CCD for substantial portions of its history, and thus contains highly variable binary lithologies ranging from nannofossil ooze/chalk, where the CaCO_3 content ranges from 92 wt% (calcareous ooze) to $<1 \text{ wt}\%$ CaCO_3 (clay).

By implementing the Simple NGR Proxy method in Hole U1583C (i.e., without interpolation or density correction), we found excellent data correlation when we manually picked the NGR values closest to the CaCO_3 content depths ($R^2 = 0.96$; 1σ of 4.19%, text-figure 2A) or interpolated NGR data to the coulometry-sampled CaCO_3 depths ($R^2 = 0.95$; 1σ of 4.41%; text-figure 2B). The Density-corrected NGR Proxy method did not substantially improve the correlation ($R^2 = 0.95$; 1σ of 4.18%; text-figure 2C, Table 2). Based on the linear regression (Eq. 7a), we constructed high-resolution estimates of CaCO_3 content through Hole U1583C (text-figure 4A), which helped us separate lithology into clay ($>50\%$ clay), clayey calcareous ooze (50%–25% clay), calcareous ooze with clay (25%–10% clay), and calcareous ooze ($<10\%$ clay).

In contrast, correcting for density changes in Hole U1557B allowed us to more substantially increase the confidence of the correlation: R^2 value changed from 0.73 (1σ of 17.82%; text-figure 3A) when we manually picked the NGR cps values (Simple NGR Proxy), to 0.75 (1σ of 16.97%; text-figure 3B) with interpolated NGR cps values (Simple NGR Proxy), and, finally, to 0.76 (1σ of 16.20%; text-figure 3C, Table 2) when sediment density and compaction were taken into account (NGR cps/g; Density-corrected NGR Proxy). Based on the linear regression (Eq. 7b), we constructed a high-resolution proxy record of CaCO_3 content through Hole U1557B (text-figure 4B). Like for U1583C, this record served to enhance the accuracy of defining sediment lithology, ranging from clay to calcareous ooze. Moreover, this record allowed a more precise calibration of the CaCO_3 content in smear slides. The sediment component contents determined by shipboard sedimentologists using smear slides from Holes U1557B (Exp. 390C) and U1583C (Exp. 393) were overestimated. On average, they were overestimated by approx. 6% with a standard deviation (1σ) of 23.2% for Hole U1557B and underestimated by about 1% with a standard deviation (1σ) of 3.9% for Hole U1583C when compared to NGR-estimated values. However, occasionally, where sediment was disturbed and the density values were unreliable, the density correction resulted in outliers, especially due to sediment loss, fracturing, biscuiting, expansion, and the switch from APC to XCB drilling (sediment disturbances), where there was a noticeable difference in the quality of fit/outlier frequency. Such disturbed intervals should be closely monitored and excluded from the calculations. More often, normalization by density compensates for irregularities and porosity changes in the cores because both bulk density and NGR are measured on the same core sections and the irregularities cancel out (Walczak et al. 2015).

Based on all CaCO_3 data collected during Expeditions 390C, 395E, 390, and 393 (seven sites and 292 data points), we constructed a cross-plot of coulometry-derived CaCO_3 content vs NGR-based



TEXT-FIGURE 4
High-resolution NGR-based CaCO_3 content (wt%) records for Holes U1583C (A) and U1557B (B) and criteria used shipboard during IODP Expeditions 390 and 393 to identify clay content and classify the sediments (Clay: >50%, Clayey: 50%–25%, with clay (wClay): 25%–10%, and no clay (Ooze): 10%–0%). Note different vertical scales in use for U1583C (A) and U1557B (B).

CaCO₃ content for marine sediments containing varying amounts of calcareous ooze and clay along the SAT. Using linear regression analysis of this data compilation, we derived the following equation for the SAT sediments (Eq. 8; text-figure 5):

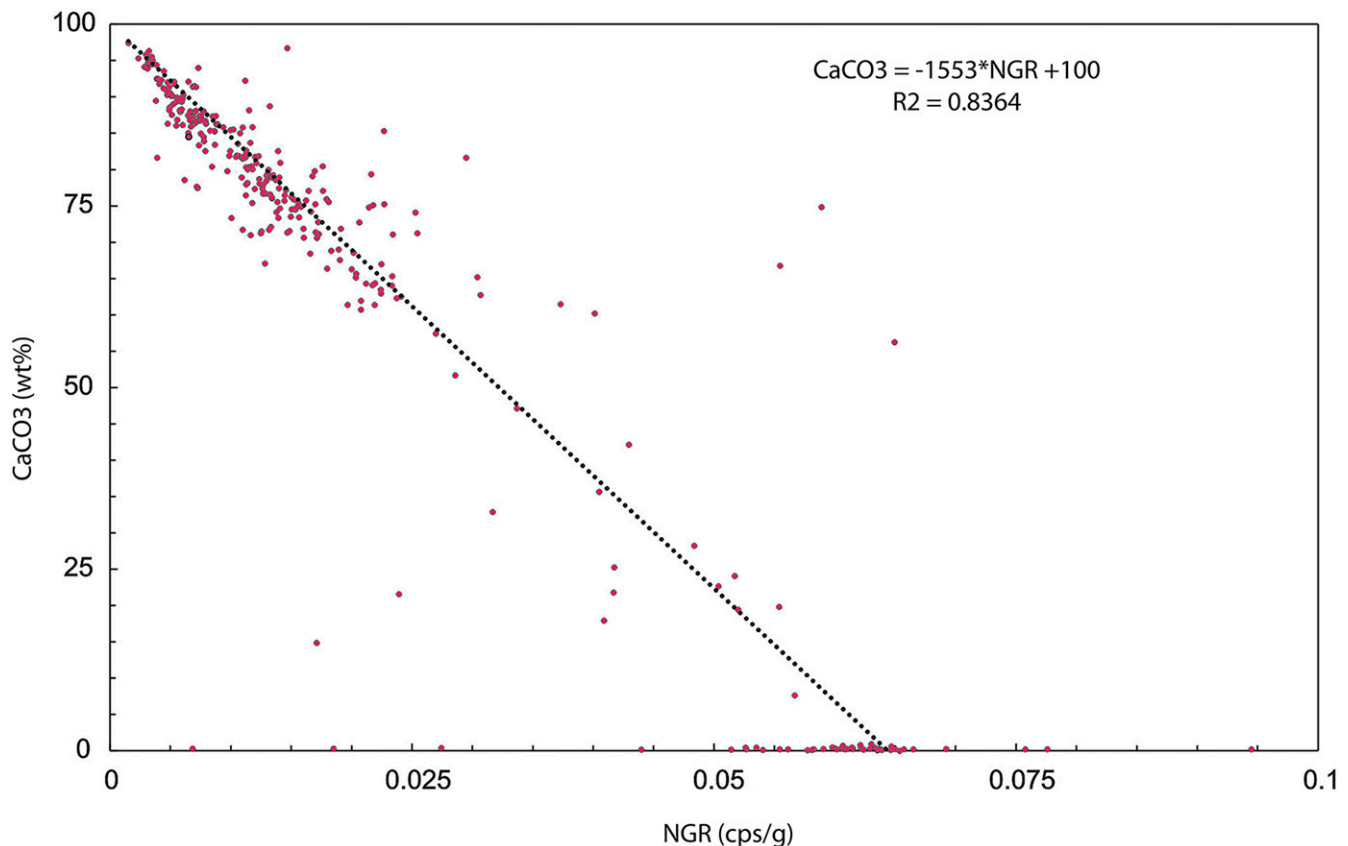
$$(8) \text{CaCO}_3 = -1553 \cdot \text{NGR} + 100 \quad (R^2 = 0.84)$$

where the CaCO₃ proxy is in wt%, and the density-normalized NGR values are in cps/g.

This is a preliminary calibration and should be tested extensively with direct measurements of carbonate content. Eq. 8 only describes seven core sites along the SAT and should not be directly applied to other deep-water IODP sites. Instead, a similar approach can be applied to NGR, GRA, and porosity data representative of another location to derive a correlation similar to Eq. 8.

As a note of caution, other factors may need to be taken into account when applying this composite regression. Some examples include percentages of different clay minerals in the terrigenous fraction, types of clay, other non-radioactive minerals in the siliciclastic fraction, organic matter content, the presence of biosilica, etc. The proposed method may not be suitable for certain oceanic environments due to various factors. These include 1) volcanic arcs and volcanic islands (hotspots) with the deposition

of low-density sediments like ash, lapilli, tuff, tuffaceous mud, pumice (e.g., Druitt et al. 2022); 2) depositional environments with high organic matter productivity, such as sapropels and organic-rich muds (e.g., Betzler et al. 2016; Druitt et al. 2022; Grant et al. 2022; Young et al. 2021); 3) intervals characterized by slope instability (extensive slumps); 4) sediments with abundant high-density metallic particles or pyrite (e.g., Hodell et al. 2023); 5) thick biosiliceous-rich units like radiolarian or diatom ooze and diatomite (Gohl et al. 2019; McKay et al. 2018); and 6) studies correlating different depositional environments or basins with variable positions of CCD or lysocline. Changes in sediment source and composition may also introduce errors in this proxy. This can relate to distance from shore and shifts in fluvial vs. aeolian flux (i.e., wet vs. dry climate in the sediment source area). Furthermore, with thorium (Th), uranium (U), and potassium (K) being primarily responsible for the produced GR energy spectrum, various clay minerals influence NGR readings differently. For example, illite is more radioactive (250–300 gAPI) than montmorillonite (150–200 gAPI), chlorite (180–250 gAPI), or kaolinite (80–130 gAPI), because it contains more K (Schlumberger 1997). If the rock matrix or formation fluids forming the clay were enriched in U or the sediments containing abundant organics, then the NGR readings would be substantially higher (Serra et al. 1980). In other cases, high K content of muscovite (~270 gAPI), biotite (~275 gAPI) (Schlumberger 1997), or other minerals (e.g., glauconite), could potentially affect the accuracy of the given



TEXT-FIGURE 5

A compilation of representative data from IODP sites U1556A, U1556C, U1557B, U1558A, U1558F, U1559A, U1560A, and U1583C showing coulometry-derived CaCO₃ content (wt%) vs NGR-based CaCO₃ content (cps/g). The linear regression has an R-squared of 0.84.

equation (Eq. 8) and its applicability to other regions of the globe. Indeed, in some depositional environments, K cannot be used to quantify clay content, as it is carried by other minerals and this is why some researchers prefer to use the combination of Th and U to obtain clay content (Day-Stirrat et al. 2021).

CONCLUSIONS

We developed a method to calculate high-resolution records of sediment CaCO_3 content based on NGR, GRA, and porosity data obtained onboard the *JOIDES Resolution*. It is based on the long-standing petrophysical observation that sedimentary clay content can be estimated from NGR values and previous observations that NGR is inversely related to carbonate content in deep-sea drilling cores. We tested both Simple and Density-corrected NGR Proxy approaches on sediment cores from the SAT (IODP Expeditions 390, 390C, 393, and 395E) and generated a robust estimate of CaCO_3 content both for homogenous lithologies at sites where the CCD remained below the seabed depth and for varied binary sediment types found at sites where the CCD fluctuated above and below the seabed depth. This method can potentially be used to improve the resolution of records of sediment CaCO_3 at other deep-ocean sites, and, hence, to refine reconstructions of paleoenvironmental and climatic changes based on such records.

ACKNOWLEDGEMENTS

This research used samples and data provided by the IODP (International Ocean Discovery Program; <https://www.zenodo.org/communities/iodp>). The authors thank the USA NSF (National Science Foundation), the FCT (Portuguese), and IODP France (French) National Funding Agencies. We are also grateful to the technical personnel, drillers, and crew of the *JOIDES Resolution*, without whom this data would not exist.

SOUTH ATLANTIC TRANSECT IODP EXPEDITION 390 AND 393 SCIENTISTS

Aizawa, M., Albers, E., Amadori, C., Belgrano, T.M., Borrelli, C., Bridges, J.D., Carter, E.J., Christeson, G.L., Coggon, R., D'Angelo, T., Dinarès-Turell, J., Doi, N., Estep, J.D., Estes, E.R., Evans, A., Garnsworthy, M., Gilhooly, W.P., III, Grant, L., Guérin, G.M., Guertin, L., Harris, M., Hojnacki, V.M., Hong, G., Jin, X., Jonnalagadda, M., Kaplan, M.R., Kempton, P.D., Kurz, W., Kuwano, D., Labonte, J.M., Lam, A.R., Latas, M., Lowery, C.M., Lu, W., McIntyre, A., Moal-Darrigade, P., Peixoto, T., Pekar, S.F., Prakasam, M., Reece, J., Robustelli Test, C., Routledge, C.M., Ryan, J.G., Santiago Ramos, D., Shchepetkina, A., Slagle, A.L., Sylvan, J.B., Takada, M., Tamborrino, L., Teagle, D.A.H., Villa, A., Wang, Y., Wee, S.Y., Widlansky, S.J., Williams, T.J., Yang, K., Tian, L., Yu, T., and Zhang, G.

REFERENCES

BECKER, K., AUSTIN, J., EXON, N., HUMPHRIS, S., KASTNER, M., MCKENZIE, J., MILLER, K., SUYEHIO, K., TAIRA, A. and UNIVERSITY OF MIAMI, 2019. Fifty years of scientific ocean drilling. *Oceanography*, 32: 17–21.

BERGER, W. H., 1972. Deep sea carbonates: Dissolution facies and age-depth constancy. *Nature*, 236: 392–395.

BETZLER, C. G., EBERLI, G. P., ALVAREZ ZARIKIAN, C. A., and THE EXPEDITION 359 SCIENTISTS. 2016. Expedition 359

preliminary report: Maldives monsoon and sea level. International Ocean Discovery Program, 16 pp.

BRALOWER, T. J., PREMOLI SILVA, I. and MALONE, M. J., 2002. Leg 198 Summary. *Proceedings of the Ocean Drilling Program, Initial Reports*, 198: 148 pp.

BURNETT, W. C., ROE, K. K. and PIPER, D. Z., 1983. Upwelling and phosphorite formation in the ocean. In: Seuss, E. and Thiede, J., Eds., *Coastal upwelling its sediment record: Part A: Responses of the sedimentary regime to present coastal upwelling*, NATO Conference Series, Series IV, Marine Sciences, 10a, 377–397. Boston: Springer US.

CHANEY, R. C., SLONIM, S. M. and SLONIM, S. S., 1982. Determination of calcium carbonate content in soils. In: Demars, K. R. and Chaney, R. C., Eds. *Geotechnical properties behavior and performance of calcareous soils, ASTM STP*, 777: 3–15. Philadelphia: American Society for Testing and Materials.

COGGON, R. M., CHRISTESON, G. L., SYLVAN, J. B., TEAGLE, D. A. H., ESTES, E., WILLIAMS, T. and ZARIKIAN, A. C. A., 2020. Expedition 390/393 Scientific Prospectus: The South Atlantic Transect. International Ocean Discovery Program. 47 pp.

COGGON, R. M., SYLVAN, J. B., TEAGLE, D. A. H., REECE, J. S., CHRISTESON, G. L., ESTES, E. R. and WILLIAMS, T., 2022a. Expedition 390/393 Scientific Prospectus addendum: South Atlantic Transect. International Ocean Discovery Program. 10 pp.

COGGON, R. M., SYLVAN, J. B., TEAGLE, D. A. H., REECE, J., CHRISTESON, G. L., ESTES, E. R., WILLIAMS, T. J. and THE EXPEDITION 390 SCIENTISTS. 2022b. Expedition 390 Preliminary Report: South Atlantic Transect 1. International Ocean Discovery Program. 62 pp.

DADEY, K. A. and LYLE, M., 1995. Development of a high-resolution calcium carbonate stratigraphy from logging data. *Proceedings of the Ocean Drilling Program, Scientific Results*, 138: 25–30.

DAGRA DATA DIGITIZER. 2022. Linear Interpolation with Excel. Retrieved from July 17, 2023 <https://www.datadigitization.com/dagra-in-action/linear-interpolation-with-excel/>.

DAY-STIRRAT, R. J., HILLIER, S., NIKITIN, A., HOFMANN, R., MAHOOD, R. and MERTENS, G., 2021. Natural Gamma-Ray Spectroscopy (NGS) as a proxy for the distribution of clay minerals and bitumen in the Cretaceous McMurray formation, Alberta, Canada. *Fuel*, 288: 119513.

DRUITT, T., KUTTEROLF, S. and HÖFIG, T. W., 2022. Expedition 398 Scientific Prospectus: Hellenic arc volcanic field. International Ocean Discovery Program. 56 pp.

DUTKIEWICZ, A. and MÜLLER, R. D., 2021. The carbonate compensation depth in the South Atlantic Ocean since the Late Cretaceous. *Geology*, 49: 873–878.

ENGLEMAN, E. E., JACKSON, L. L. and NORTON, D. R., 1985. Determination of carbonate carbon in geological materials by coulometric titration. *Chemical Geology*, 53: 125–128.

ESTES, E. R., WILLIAMS, T., MIDGLEY, S., COGGON, R. M., SYLVAN, J. B., CHRISTESON, G. L. and TEAGLE, D. A. H., 2020. Expedition 390C Preliminary Report: South Atlantic Transect reentry systems. International Ocean Discovery Program. 34 pp.

FARRELL, J. W. and PRELL, W. L., 1989. Climatic change and CaCO_3 preservation: An 800,000 year bathymetric reconstruction from the central equatorial Pacific Ocean. *Paleoceanography*, 4: 447–466.

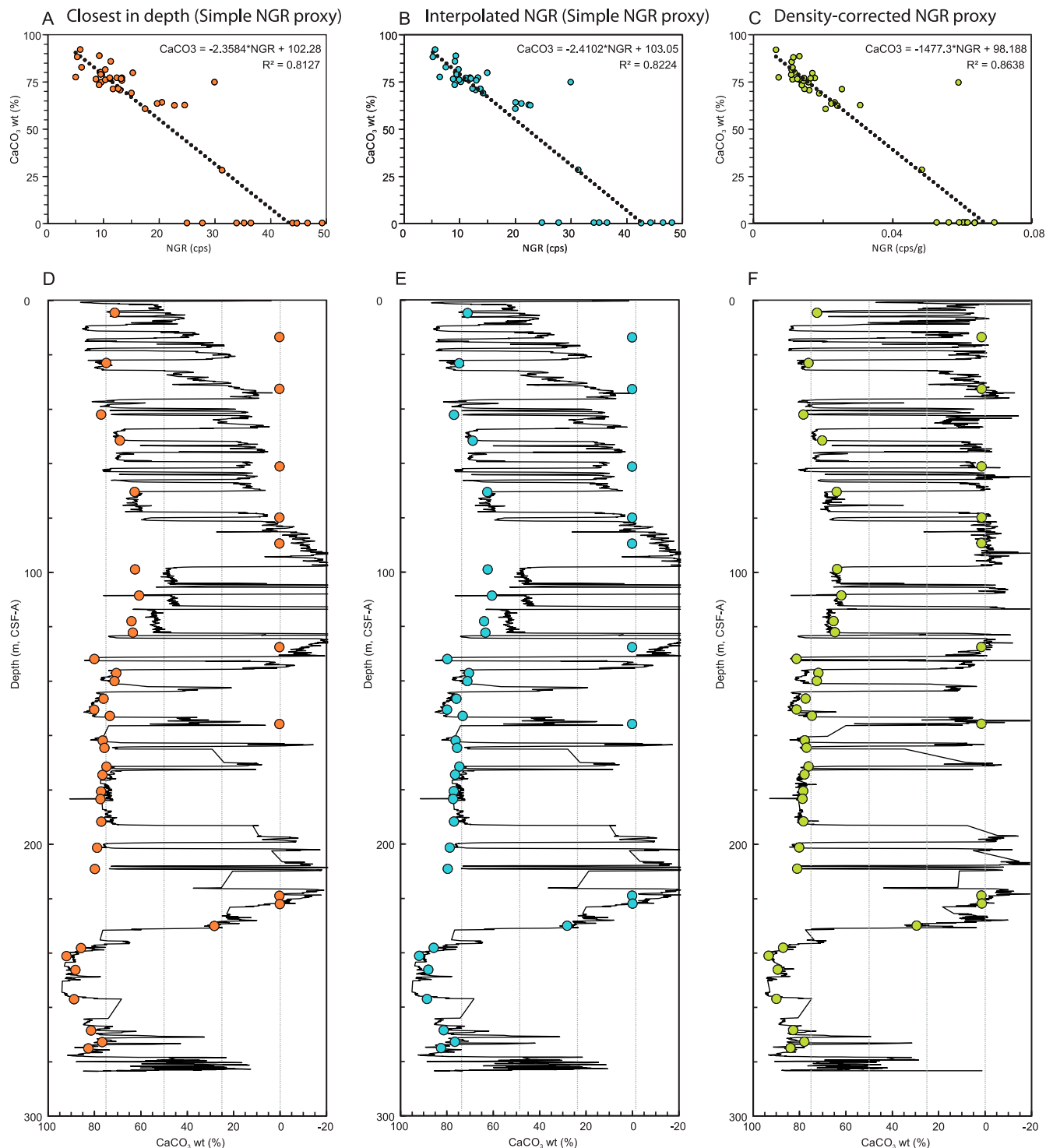
- GOHL, K., WELLNER, J. S., KLAUS, A. and THE EXPEDITION 379 SCIENTISTS. 2019. Expedition 379 Preliminary Report: Amundsen Sea West Antarctic Ice Sheet History. International Ocean Discovery Program. 33 pp.
- GRANT, K. M., AMARATHUNGA, U., AMIES, J. D., HU, P., QIAN, Y., PENNY, T., RODRIGUEZ-SANZ, L., ZHAO, X., HESLOP, D., LIEBRAND, D., HENNEKAM, R., WESTERHOLD, T., GILMORE, S., LOURENS, L. J., ROBERTS, A. P. and ROHLING, E. J., 2022. Organic carbon burial in Mediterranean sapropels intensified during Green Sahara Periods since 3.2 Myr ago. *Communications Earth and Environment*, 3: 11.
- HODELL, D. A., ABRANTES, F., ALVAREZ ZARIKIAN, C. A. and THE EXPEDITION 397 SCIENTISTS. 2023. Expedition 397 preliminary report: Iberian margin paleoclimate. International Ocean Discovery Program. 50 pp.
- HUFFMAN, E. W. D., 1977. Performance of a new automatic carbon dioxide coulometer. *Microchemical Journal*, 22: 567–573.
- JONES, G. A. and KAITERIS, P. J., 1983. A vacuum-gasometric technique for rapid and precise analysis of calcium carbonate in sediment soils. *Journal of Sedimentary Research*, 53: 655–660.
- KARDELL, D. A., CHRISTESON, G. L., ESTEP, J. D., REECE, R. S. and CARLSON, R. L., 2019. Long-lasting evolution of layer 2A in the Western South Atlantic: Evidence for low-temperature hydrothermal circulation in old oceanic crust. *Journal of Geophysical Research: Solid Earth*, 124: 2252–2273.
- KOCHENOV, A. V. and BATURIN, G. N., 2002. The paragenesis of organic matter, phosphorus, and uranium in marine sediments. *Lithology and Mineral Resources*, 37: 107–120.
- LAMY, F., WINCKLER, G., ALVAREZ ZARIKIAN, C. A. and THE EXPEDITION 383 SCIENTISTS. 2019. Expedition 383 preliminary report: Dynamics of the Pacific Antarctic circumpolar current. International Ocean Discovery Program. 81 pp.
- LINDSEY, M. M. and SCHELLENBERG, S. A., 2006. Early Eocene to Late Miocene variations in the South Atlantic CCD: Constraints from the Walvis Ridge depth-transect (ODP Leg 208). *AGU Fall Meeting Abstracts*, 2006: PP23A-1737.
- LYLE, M., MURRAY, D. W., FINNEY, B. P., DYMOND, J., ROBBINS, J. M. and BROOKSFORCE, K., 1988. The record of late Pleistocene biogenic sedimentation in the eastern tropical Pacific Ocean. *Paleoceanography*, 3: 39–59.
- MARSAGLIA, K., MILLIKEN, K. and DORAN, L., 2013. IODP digital reference for smear slide analysis of marine mud. Part 1: Methodology and atlas of siliciclastic and volcanogenic components. *IODP*, Technical Note No. 1, 263 pp.
- MARSAGLIA, K., MILLIKEN, K., LECKIE, R. M., TENTORI, D. and DORAN, L., 2015. IODP smear slide digital reference for sediment analysis of marine mud. Part 2: Methodology and atlas of biogenic components. *IODP*, Technical Note No. 2, 382 pp.
- MAYER, L. A., 1991. Extraction of high-resolution carbonate data for palaeoclimate reconstruction. *Nature*, 352: 148–150.
- MAZZULLO, J. and GRAHAM, A. G., 1988. *Handbook for shipboard sedimentologists*. Arlington: Ocean Drilling Program, Texas A&M University, Technical Note No. 8, 70 pp.
- MCKAY, R. M., DE SANTIS, L., KULHANEK, D. K. and THE EXPEDITION 374 SCIENTISTS. 2018. Expedition 374 preliminary report: Ross Sea West Antarctic ice sheet history. International Ocean Discovery Program. 63 pp.
- MELGUEN, M., 1978. Facies evolution, carbonate dissolution cycles in sediments from the eastern South Atlantic (DSDP Leg 40) since the Early Cretaceous. *Initial Reports of the Deep Sea Drilling Project*, 60: 543–586.
- MILLWOOD, L. D., HAWKINS, D. L., JR and WELLS, S. M., 2002. Data report: Utilizing color reflectance analysis as a carbonate concentration proxy. *Proceedings of the Ocean Drilling Program, Scientific Results*, 181: 1–50.
- PEDERSEN, T. F., 1983. Increased productivity in the eastern equatorial Pacific during the last glacial maximum (19,000 to 14,000 yr BP). *Geology*, 11: 16–19.
- PHILLIPS, S. C. and LITTLER, K., 2022. Comparison of sediment composition by smear slides to quantitative shipboard data: A case study on the utility of smear slide percent estimates. *IODP Expedition 353, northern Indian Ocean. Scientific Drilling*, 30: 59–74.
- PIMMEL, A. and CLAYPOOL, G., 2001. Introduction to shipboard organic geochemistry on the *JOIDES Resolution*. ODP, Technical Note No. 30, 29 pp.
- PRATSON, E. L., BROGALIA, C., MOLINIE, A. and ABRAMS, L., 1992b. 34. Data report: Geochemical well logs through Cenozoic sediments from sites 800, 801, and 802. *Proceedings of the Ocean Drilling Program, Scientific Results*, 129: 635–651.
- PRATSON, E. L., HOBART, M. and BROGLIA, C., 1992a. 39. Data report: Results of geochemical well logging in the Izu-Bonin forearc basin, Sites 782 and 786, Leg 125. *Proceedings of the Ocean Drilling Program, Scientific Results*, 125: 663–673.
- PRATSON, E. L., LYLE, M. and TIVY, J., 1993. 48. Data report: Geochemical well logs through Cenozoic sediments from Sites 805 and 806. *Proceedings of the Ocean Drilling Program, Scientific Results*, 130: 775–788.
- RIDER, M. H., 1996. *The geological interpretation of well logs* (2nd ed.). Sucherland: Rider-French Consulting Ltd, 175 pp.
- ROTHWELL, R. G. and RACK, F. R., 2006. New techniques in sediment core analysis: An introduction. *Geological Society, London, Special Publications*, 267: 1–29.
- SCHLUMBERGER. 1997. *Log interpretation charts*. Houston: Schlumberger Wireline and Testing, 310 pp.
- SERRA, O., BALDWIN, J. and QUIREIN, J., 1980. Theory, Interpretation, and Practical Applications of natural gamma ray spectroscopy. *SPWLA 21st annual logging symposium*.
- TEAGLE, D. A. H., REECE, J., COGGON, R. M., SYLVAN, J. B., CHRISTESON, G. L., WILLIAMS, T. J., ESTES, E. R. and THE EXPEDITION 393 SCIENTISTS. 2023. Expedition 393 preliminary report: South Atlantic transect 2. International Ocean Discovery Program (IODP), 80 pp.
- TELFORD, W. M., GELDART, L. P., SHERITT, R. E. and KEYS, D. A., 1976. *Applied geophysics*. Cambridge: Cambridge University Press, 860 pp.
- VAN ANDEL, T. H., 1975. Mesozoic/Cenozoic calcite compensation depth and the global distribution of calcareous sediments. *Earth and Planetary Science Letters*, 26: 187–194.
- VASILIEV, M. A., BLUM, P., CHUBARIAN, G., OLSEN, R., BENNIGHT, C., COBINE, T., FACKLER, D., HASTEDT, M.,

- HOUPT, D., MATEO, Z. and VASILIEVA, Y. B., 2011. A new natural gamma radiation measurement system for marine sediment and rock analysis. *Journal of Applied Geophysics*, 75: 455–463.
- VEEH, H. H., CALVERT, S. E. and PRICE, N. B., 1974. Accumulation of uranium in sediments and phosphorites on the south west African shelf. *Marine Chemistry*, 2: 189–202.
- WALCZAK, M. H., MIX, A. C., WILLSE, T., SLAGLE, A., STONER, J. S., JAEGER, J., GULICK, S., LEVAY, L., KIOKA, A. and THE IODP EXPEDITION 341 SCIENTIFIC PARTY. 2015. Correction of non-intrusive drill core physical properties data for variability in recovered sediment volume. *Geophysical Journal International*, 202: 1317–1323.
- WILLIAMS, T., ESTES, E. R., RHINEHART, B., COGGON, R. M., SYLVAN, J. B., CHRISTESON, G. L. and TEAGLE, D. A. H., 2021. Expedition 395E preliminary report: Complete south Atlantic transect reentry systems. International Ocean Discovery Program. 34 pp.
- YOUNG, J. R., ARCHONTIKIS, O. A., SU, X. and PRATIWI, S. D., 2021. Nannofossil palaeoecology of lower Miocene sapropels from IODP Expedition 359, the Maldives. *Palaeogeography, Palaeoclimatology, Palaeoecology*, 571: 110325.
- ZENODO. Zenodo IODP database. International Ocean Discovery Program. http://publications.iodp.org/proceedings/390_393/datasets.html. Accessed on September 4, 2024.

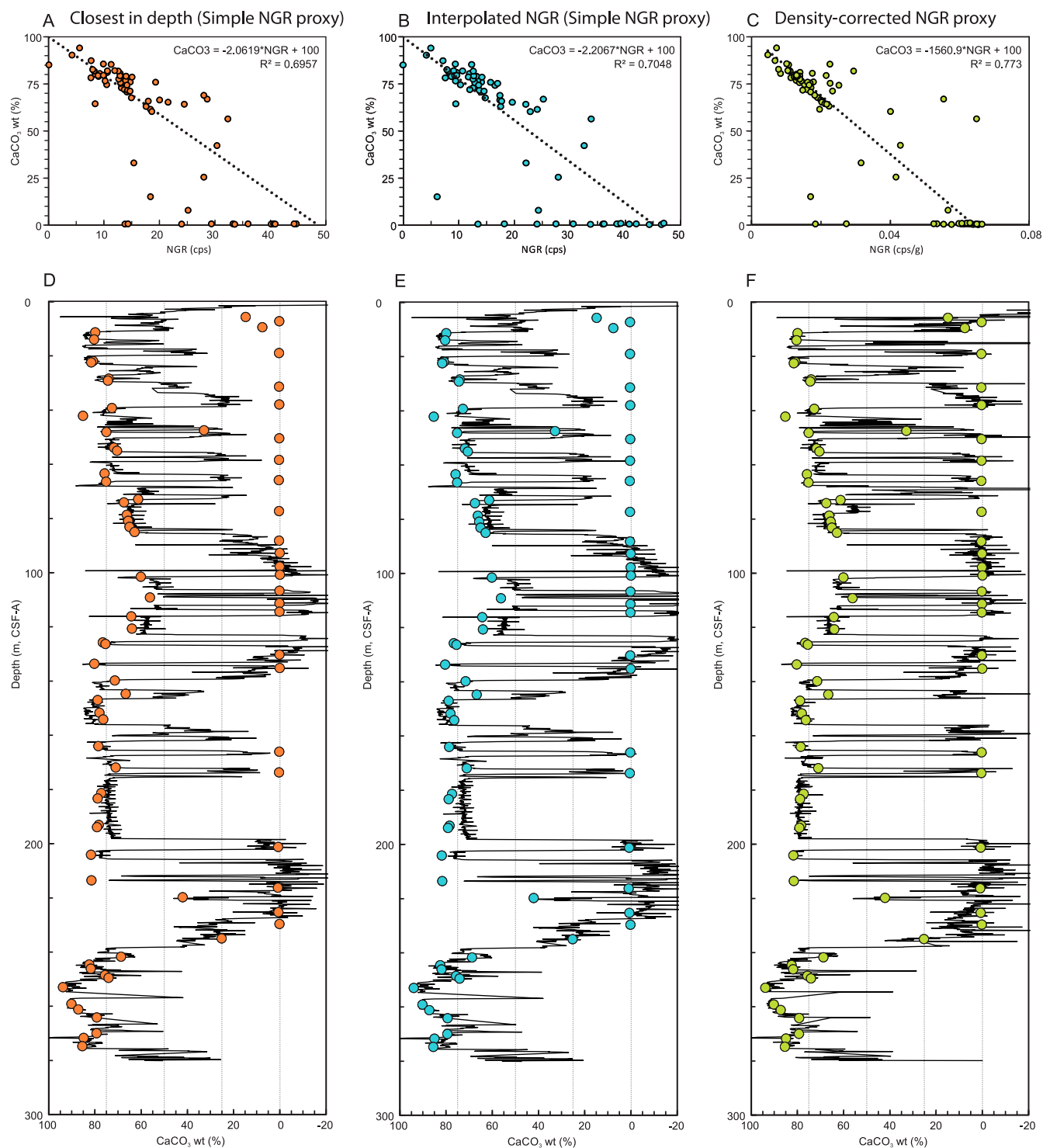
APPENDIX

(A-C) Cross-plots of coulometry-derived CaCO_3 content (wt%) vs. NRG counts (cps) for other IODP sites (U1556A, U1556C, U1558A, U1558F, U1559A, U1560A, and U1583C) with linear regression equations and R^2 values. In linear regression equations, y is the CaCO_3 content in wt%, and the NRG values are in cps or

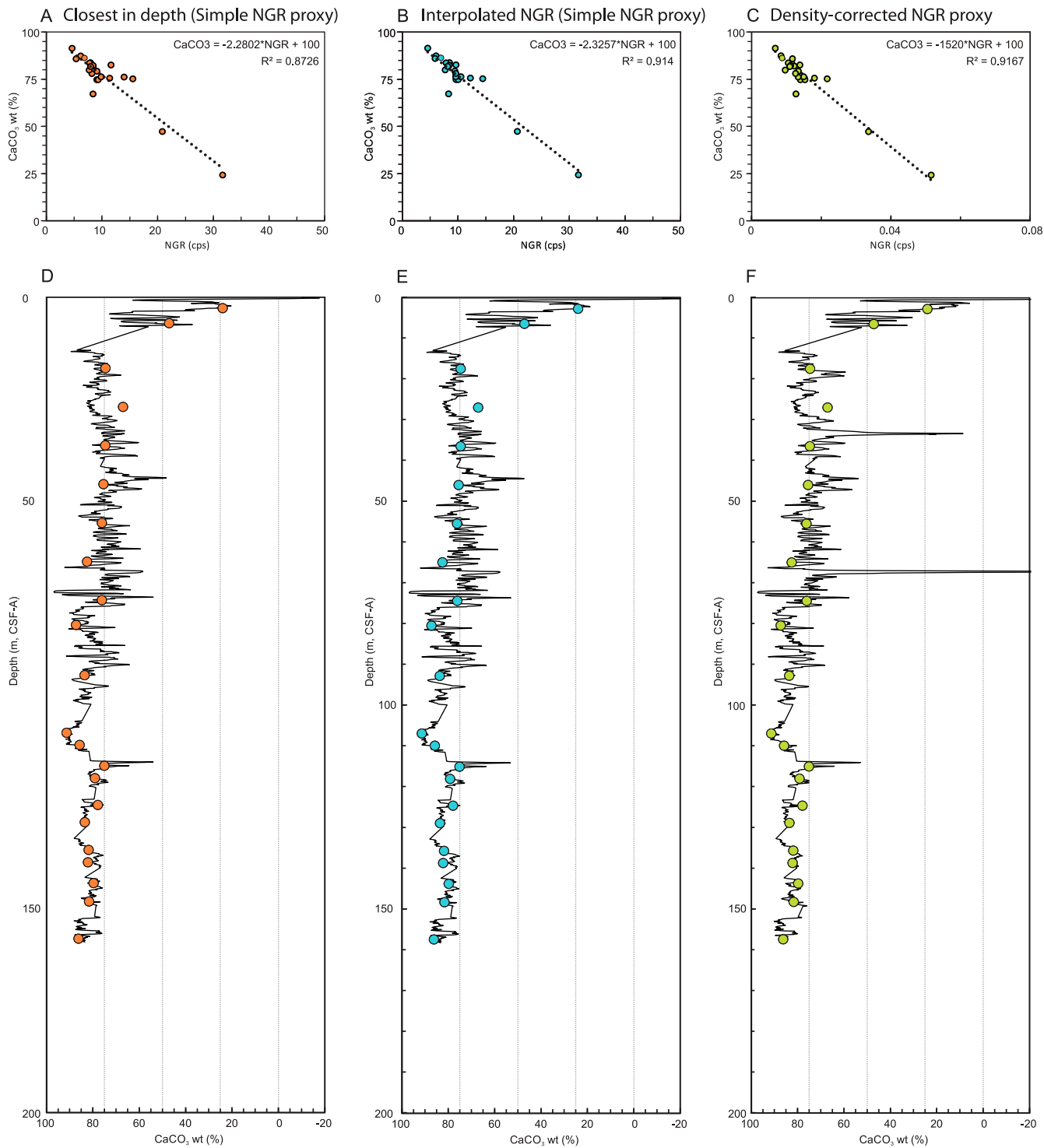
cps/g. (D-F) NRG-based CaCO_3 content (wt%) records synthesized from the application of three different NRG– CaCO_3 content calibrations (A–C) to the approx. 10 cm resolution for other IODP sites (U1556A, U1556C, U1558A, U1558F, U1559A, U1560A, and U1583C).



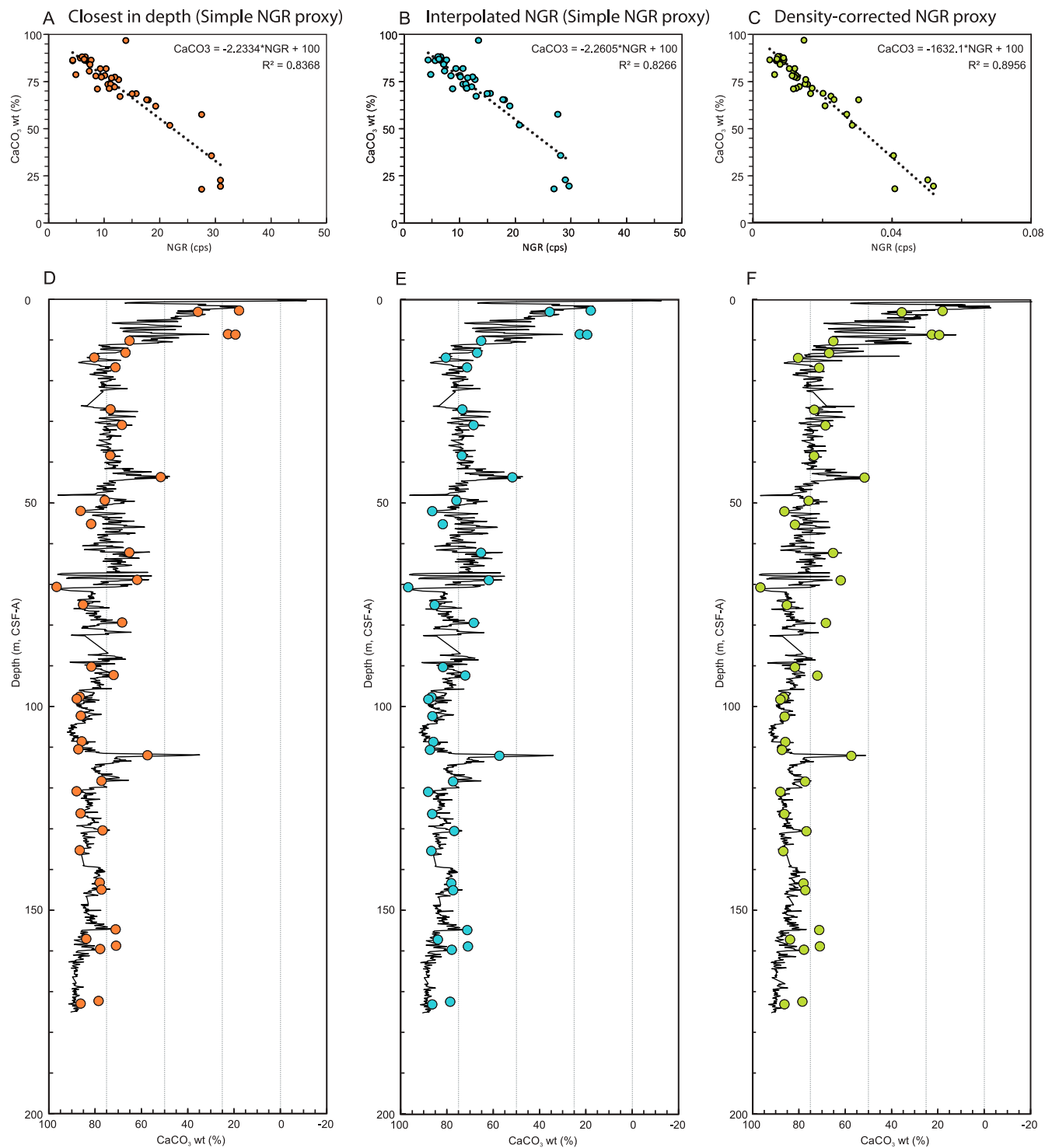
Hole U1556A



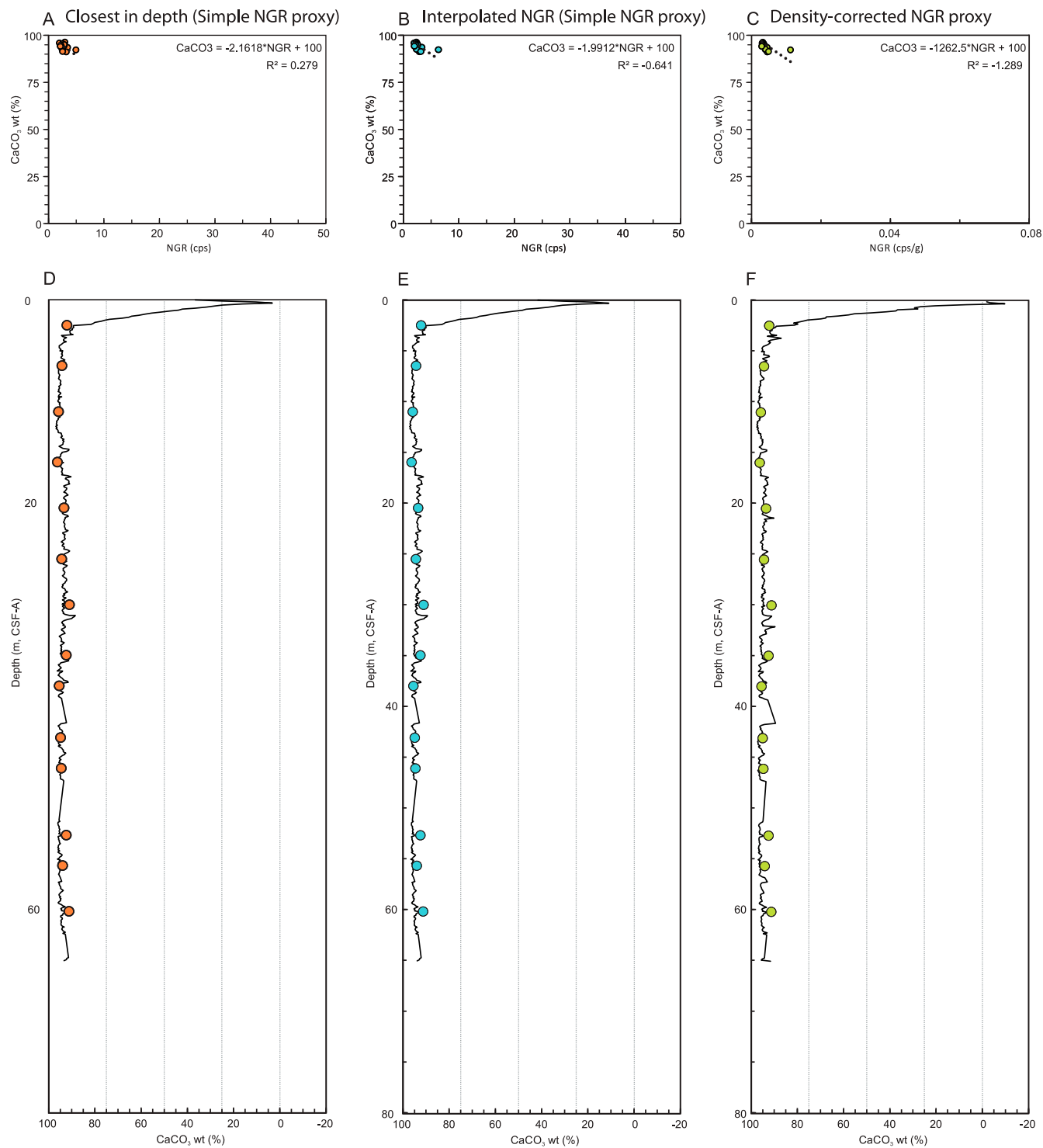
Hole U1556C



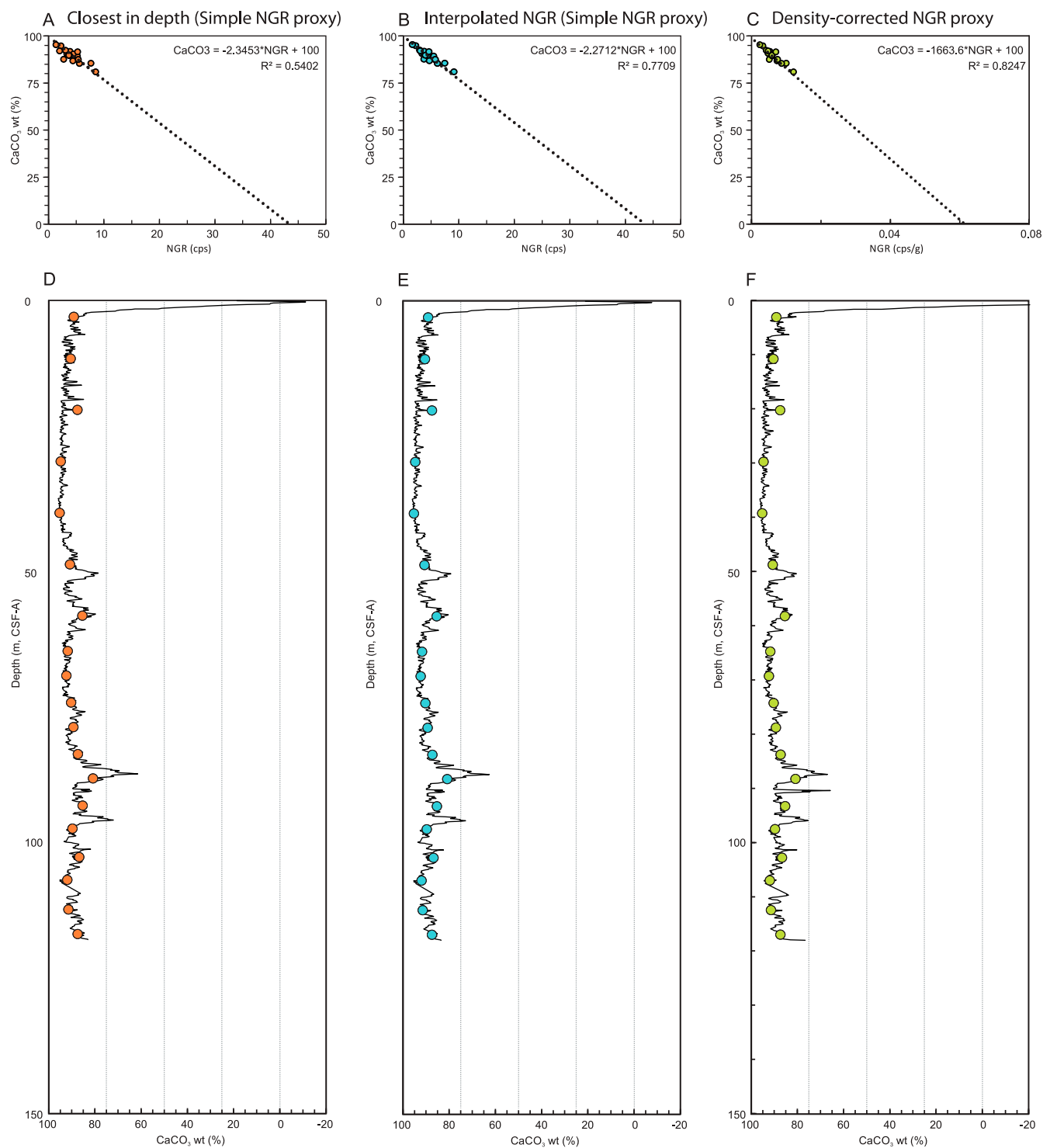
Hole U1558A



Hole U1558F



Hole U1559A



Hole U1560A